Scientific Reports

https://doi.org/10.1038/s41598-026-59546-z

Article in Press

CuO/ZnO nanocomposites synthesized using *Ensete ventricosum* extract: antibacterial and antioxidant activity

Received: 3 March 2026

Accepted: 22 June 2026

Published online: 13 July 2026

Cite this article as: Gebremichael T.E., Adula S.H., Bassa A.B. *et al.* CuO/ZnO nanocomposites synthesized using *Ensete ventricosum* extract: antibacterial and antioxidant activity. *Sci Rep* (2026). https://doi.org/10.1038/s41598-026-59546-z

Tekileab Engida Gebremichael, Shemelis Hailu Adula, Atinafu Bergene Bassa, Chalachew Mesfin Tafere, Tamirat Engida Gebremikael, Zerfu Haile Robi, Alemayehu Workiye Haile & Endale Tesfaye

CuO/ZnO nanocomposites synthesized using *Ensete ventricosum* extract: antibacterial and antioxidant activity

Tekileab Engida Gebremichael[1*], Shemelis Hailu Adula[1], Atinafu Bergene Bassa[1], Chalachew Mesfin Tafere[1], Tamirat Engida Gebremikael[2,3], Zerfu Haile Robi[4], Alemayehu Workiye Haile[5], Endale Tesfaye[1]

[1]Chemistry Department, Gambella University, Gambella, Ethiopia. ORCID (Tekileab Engida Gebremichael): https://orcid.org/0009-0004-1711-7210

[2]Mechanical Engineering Department, FDRE Technical and Vocational Training Institute (FTVTI), Addis Ababa, Ethiopia

[3]Department of Mechanical Engineering, Shisho Inde TVET College, Bonga, Ethiopia

[4]Chemistry Department, Oda Bultum University, Ciro, Ethiopia

[5]Nursing Department, Mattu University, Mattu, Ethiopia

[*]Corresponding authors: E-mail: tekileab2009@gmail.com, tekileab@gmu.edu.et

Abstract

Most infection-causing pathogens have developed resistance to conventional antibiotic treatments, while free radicals can also induce cellular damage by disrupting essential biomolecules and cellular structures. Binary metal oxide nanocomposites have attracted increasing attention due to their unique physicochemical properties, enhanced stability, and superior biological and catalytic performance compared to single metal oxides.

In this study, CuO/ZnO nanocomposites were successfully synthesized via a green, eco-friendly approach using *Ensete ventricosum* leaf extract, yielding well-defined heterostructures with enhanced biological performance relative to the individual oxides. The UV-Vis spectrum showed an absorption peak at

421 nm with a band gap energy of 3.25 eV, which is slightly lower than that of pure ZnO, indicating a strong interaction between CuO and ZnO phases. The crystallite size was found to be 24.5 nm from XRD analysis, confirming the nanocrystalline nature of the material. FT-IR analysis confirmed the presence of Zn–O and Cu–O stretching vibrations at 545 and 560 cm^{-1}, respectively. SEM analysis revealed slightly agglomerated particles, while EDS confirmed the presence of Zn, Cu, and O elements.

The synthesized CuO/ZnO nanocomposites exhibited significant antibacterial activity against *Staphylococcus aureus* (22.64 mm) and *Escherichia coli* (19.21 mm), along with strong antioxidant activity ($IC_{50} \approx 107.18$ µg/mL), compared with CuO NPs (~150 µg/mL) and ZnO NPs (~180 µg/mL) in DPPH radical scavenging assays. These results demonstrate that the CuO/ZnO heterojunction enhances biological activity. This work provides a scalable green synthesis strategy for CuO/ZnO NCs with promising antimicrobial and antioxidant applications, highlighting the potential of plant-mediated routes for environmentally friendly nanomaterial synthesis.

Keywords: CuO/ZnO NCs, DPPH, Green synthesis, *Ensete ventricosum*

Introduction

Most infection-causing pathogens are resistant to conventional antibiotic treatment [1]. In addition, free radicals can induce cellular damage by disrupting essential biomolecules [2]. Metal oxide nanoparticles have therefore attracted considerable attention due to their unique physicochemical properties, such as high surface area, tunable electronic structure, and intrinsic antibacterial activity [3]. Among them, CuO and ZnO nanoparticles are widely studied for their strong antimicrobial properties, chemical stability, and availability [4]. In particular, CuO/ZnO nanocomposites offer synergistic advantages and have shown enhanced antimicrobial performance in various microbial studies.

Concerns related to safety and environmental impact arise from the use of hazardous chemicals, high temperatures, and energy-intensive processes in conventional methods for synthesizing metal oxide nanoparticles [5]. Green synthesis offers an eco-friendly alternative by utilizing plant extracts as reducing and stabilizing agents derived from natural biomolecules such as sugars, flavonoids, and polyphenols [6]. In this context, *Ensete ventricosum* (Enset), an important perennial plant widely cultivated in Ethiopia for food production (Kocho) and traditional uses, represents a promising bioresource. In this study, leaves were collected from Gesha Woreda, Kefa Zone, Ethiopia, an area known for its rich biodiversity and extensive Enset cultivation[7, 8]. These leaves contain bioactive compounds that can facilitate the green synthesis of nanomaterials, offering a cost-effective and sustainable route for producing functional nanocomposites[9, 10]. However, despite its potential, limited studies have investigated the use of Enset leaf extract for the synthesis of CuO/ZnO NCs with antimicrobial activity.

Through synergistic interactions at the heterojunction interface, the combined use of ZnO and CuO in a binary NCs can significantly enhance functional properties [11]. Compared with their individual counterparts, CuO/ZnO nanocomposites are reported to exhibit improved charge separation, increased reactive oxygen species (ROS) generation, and enhanced antibacterial activity [12]. In addition, their redox-active surfaces may also contribute to antioxidant behavior depending on the environmental conditions, enabling dual functional applications [13]. Although green synthesis of metal oxide nanomaterials using plant extracts has been widely reported, studies on CuO/ZnO nanocomposites derived from *Ensete ventricosum* leaf extract remain limited. This work, therefore provides a distinct contribution through a systematic comparative evaluation of the functional properties of the synthesized NCs

In this work, we report a facile and eco-friendly synthesis of CuO/ZnO NCs using this plant extract as both reducing and stabilizing agent. The novelty of this study lies in the formation of a heterostructured composite with enhanced functional properties, together with a comparative evaluation of its antibacterial and antioxidant performance against corresponding individual oxides [14]. The synthesized NCs were systematically characterized using FTIR, XRD, SEM, EDX, and UV–Vis spectroscopy. The antioxidant capacity was evaluated using a standard radical scavenging assay, while antibacterial performance was assessed against Gram-negative *Escherichia coli* and Gram-positive *Staphylococcus aureus.* Overall, this study investigates the relationship between green-mediated synthesis, interfacial heterostructure formation, and dual functional (antibacterial and antioxidant) activity, highlighting the potential of CuO/ZnO NCs as environmentally friendly antimicrobial materials.

Materials and Methods

Chemicals and reagents

Chemicals used in this study including Zinc nitrate hexahydrate ($Zn(NO_3)_2 \cdot 6H_2O$, 99% Sigma-Aldrich, Germany), Copper nitrate trihydrate ($Cu(NO_3)_2 \cdot 3H_2O$, 99% Sigma-Aldrich, Germany), Sodium hydroxide (NaOH, 98% Merck, Germany) and Ethanol (C_2H_5OH, 99.5% Sigma-Aldrich, Germany) were used for the production of binary nanocomposite in the study. All chemicals were used without further purification. Deionized water was used throughout the experiment.

Enset (*Ensete ventricosum*) Leaf Extract Preparation

The preparation of the plant extract was completed using the procedure outlined in Ref. [15, 16] with minor modifications.

Fresh Enset (*Ensete ventricosum*) leaves were collected from the surroundings of a local Gesha Woreda, located in the Kefa Zone of Ethiopia. The plant species was identified based on its well-known morphological characteristics and comparison with published botanical descriptions of *Ensete ventricosum*. Since the plant is a commonly cultivated species in Ethiopia, no formal identification by a taxonomist was required[8]. As the plant is widely cultivated and collected from publicly accessible areas, no specific permits were required according to local regulations. The leaves were thoroughly cleaned of dust and contaminants using distilled water. Then allowed to air dry for 48 hours at room temperature. The collected leaves were thoroughly washed with distilled water and air-dried at room temperature for 48 hours. The dried leaves were then chopped into small pieces and boiled in distilled water (10 g per 100 mL) at 80 °C for 30 min. The obtained aqueous extract was filtered.

CuO NPs Synthesis

CuO NPs were successfully synthesized via a green approach using plant extract as both reducing and stabilizing agents, based on the procedure reported in Ref. [17, 18] with slight modifications.

A 0.1 M aqueous solution of copper(II) sulfate pentahydrate ($CuSO_4 \cdot 5H_2O$) was prepared by dissolving 1.25 g of $CuSO_4 \cdot 5H_2O$ in 50 mL of distilled water under constant stirring at 60 °C. Subsequently, 25 mL of *Ensete ventricosum* extract was added dropwise to the solution under continuous stirring. The pH of the mixture was adjusted to 10 using 2 M NaOH solution, resulting in the formation of a dark brown precipitate. The reaction mixture was further stirred at 70 °C to ensure complete reaction and homogeneity. The resulting precipitate was collected and washed three times with distilled water followed by ethanol to remove impurities. The product was then dried at 80 °C for 3 hours and finally calcined at 350 °C to enhance crystallinity and obtain pure CuO NPs.

ZnO NPs Synthesis

Similar green synthesis methods were used to synthesize ZnO NPs following the method reported in Ref. [19, 20] with slight modifications.

A 0.1 M zinc acetate dihydrate solution ($Zn(CH_3COO)_2 \cdot 2H_2O$) was prepared by dissolving 1.10 g of zinc acetate dihydrate in 50 mL of distilled water under constant stirring. After that, 25 mL of Enset (*Ensete ventricosum)* leaf extract was added while being constantly stirred. 1 M NaOH was used to bring the pH to 10. The reaction mixture was further stirred at 70 °C to ensure complete reaction and homogeneity. The resulting precipitate was collected and washed three times with distilled water followed by ethanol to remove impurities. The product was then dried at 80 °C for 3 hours and finally calcined at 350 °C to enhance crystallinity and obtain pure ZnO NCs.

CuO/ZnO NCs Synthesis

The CuO/ZnO binary metal oxide NCs were synthesized by a green, one-pot approach using *Ensete ventricosum* extract as a natural reducing and stabilizing agent. CuO/ZnO NCs were successfully synthesized following the method reported in Ref. [21, 22] with slight modifications.

Aqueous solutions of $Cu(NO_3)_2 \cdot 3H_2O$ and $Zn(NO_3)_2 \cdot 6H_2O$ were prepared separately at a concentration of 0.1 M using distilled water. The precursor solutions were then mixed in a Cu:Zn molar ratio of 1:2 under continuous magnetic stirring at 60 °C for 1 hour. For the synthesize CuO/ZnO NCs, 20 mL of *Ensete ventricosum* leaf extract was added dropwise to the mixed metal solution under continuous stirring continuously at 60 °C for 1 hour. The formation of a brownish-green precipitate indicated the progression of the reaction. The pH of the solution was adjusted at 10 using 1 M NaOH to promote complete precipitation of the nanocomposite. The resulting precipitate was collected by centrifugation at 6000 rpm for 10 minutes,

followed by repeated washing four times with distilled water and subsequently with ethanol to remove residual biomolecules and impurities. The purified product was dried at 80 °C for 3 hours and then calcined at 400 °C for 3 hours in a muffle furnace to eliminate organic residues, improve crystallinity, and enhance structural stability.

The obtained CuO/ZnO nanocomposites were subsequently characterized using X-ray diffraction (XRD), scanning electron microscopy (SEM), Fourier transform infrared spectroscopy (FTIR), and UV–Vis spectroscopy.

Method of Optimization

Reaction time, temperature, pH, Cu:Zn molar ratio, and precursor concentration were systematically varied during synthesis optimization. For each condition, UV-Vis spectra were recorded [23]. The most successful CuO/ZnO nanocomposites were selected based on several factors, including maximum peak intensity with distinct CuO and ZnO absorption features, appropriate peak shifts indicating strong interaction between the two components, high crystallinity as confirmed by X-ray diffraction (XRD), and superior antibacterial activity. These results confirm that the optimized CuO/ZnO nanocomposites are biologically active, well-dispersed, and fully formed. Among the tested conditions, the Cu molar ratio of 1:2 at 0.1 M precursor concentration, 60 °C reaction temperature, 1 h reaction time, and pH 10 produced nanocomposites with the highest antibacterial and antioxidant activity and was therefore selected for detailed characterization.

Characterization Techniques

Some methods were used to confirm the optical characteristics and structure of the produced CuO/ZnO NCs [24].

UV-Visible spectrophotometer analysis: A UV-Vis double beam spectrophotometer, the synthesized ZnO and CuO NPs and CuO/ZnO NCs

solution with deionized water carried out the initial characterization. The spectra were recorded in between wavelength range 250 nm to 600 nm. The optical band gap of the CuO/ZnO NCs was determined using the Tauc relation (Equation 1):

$$\alpha h\nu^{n} = A(h\nu - Eg) \quad \text{.....Equation 1}$$

Where:

- α = absorption coefficient
- $h\nu$ = photon energy
- A = constant
- E_g = band gap energy
- n = 1/2 for direct allowed transitions

FTIR analysis: FT-IR spectra of NPs were measured between 4000 to 400 cm^{-1}. The dried powder of ZnO, CuO and CuO/ZnO NCs was used for functional group characterizations.

XRD analysis: XRD technique was employed to identify the crystallinity, average crystalline size and composition of ZnO, CuO, and CuO/ZnO NCs, as well as their purity. The diffraction patterns were recorded to confirm phase formation and crystallinity. The average crystallite size was calculated using the Scherrer equation (Equation 2):

$$D = \frac{K\lambda}{\beta\cos\theta} \quad \text{.....Equation 2}$$

Where: D is crystallite size, $K = 0.9$ is the shape factor, $\lambda = 1.5406$ Å (Cu Kα radiation), β is the full width at half maximum (FWHM), and θ is the Bragg angle.

SEM analysis: SEM analysis was done to study the size, shape, and surface roughness of the synthesized NPs and NCs.

EDS: EDS was used to determine the elemental makeup of the produced CuO/ZnO NCs. The powdered sample was placed on conductive carbon tape and examined at energies between 0 and 12 keV. The distinctive emission peaks corresponding to the O, Cu, and Zn elements contained in the NCs were identified using the obtained spectra.

Antimicrobial Properties

The activity of the produced CuO/ZnO NCs was tested by using the disk diffusion method to determine their efficacy against *E. coli* and *S. aureus* bacterial strains according to the procedures described in the literature [25, 26].

Bacterial suspension adjusted to a 0.5 McFarland standard and uniformly spread onto nutrient agar plates using a sterile swab. Sterile paper disks (6 mm diameter) impregnated with CuO/ZnO NCs at concentrations of 25, 50, 75, and 100 µg/mL were placed onto the inoculated agar plates. Gentamicin was used as a positive control, while sterile distilled water served as a negative control. The plates were incubated at 37 °C for 24 hours. After incubation, the diameter of the inhibition zones was measured in millimeters (mm). All experiments were performed in triplicate (n = 3), and the results are presented as mean ± standard deviation. The minimum inhibitory concentration (MIC) of the synthesized CuO/ZnO nanocomposites was determined using the broth microdilution method. Serial dilutions of the nanocomposites were prepared and inoculated with bacterial suspensions. The cultures were incubated at 37 °C for 24 h. The MIC was defined as the lowest concentration of the nanocomposite that completely inhibited visible bacterial growth.

Antioxidant properties

The antioxidant properties were successfully evaluated to assess radical scavenging ability, which complements the antimicrobial activity. DPPH antioxidant activity was evaluated following the method reported in Ref. [27, 28] with slight modifications. 1 mL of CuO/ZnO NCs solution (25–200 µg/mL) was mixed with 1 mL of 0.1 mM DPPH in methanol. Ascorbic acid was used as a standard. IC_{50} values were calculated by using Equation 3.

$$\text{Scavenging \%} = \frac{\text{A control-A sample}}{\text{A control}} \times 100 \quad \text{..... Equation 3}$$

Where:

A control = absorbance of control

A sample = absorbance of sample

Statistical Analysis

All experiments related to the application studies of the CuO/ZnO nanocomposites were performed in triplicate. The obtained data are presented as mean ± standard deviation (SD). Statistical analysis was carried out using one-way analysis of variance (ANOVA), and differences were considered statistically significant at $p < 0.05$.

Results and Discussion

Optimization of Synthesis Parameters

The synthesis parameters, including Cu:Zn ratio, precursor concentration, reaction time, pH, and leaf extract volume, were systematically varied to optimize the formation of CuO/ZnO nanocomposites. UV–Vis intensity was used as the primary criterion for selection, with the highest intensity indicating optimal formation. As shown in Table 1, the Cu:Zn ratio of 1:2, precursor concentration of 0.1 M, reaction time of 1 hour, pH 10, and 20 mL leaf extract yielded the highest UV–Vis intensity (1.05 a.u.), confirming this combination as the best condition.

Table 1: Optimization of key synthesis parameters used for the preparation of CuO/ZnO nanocomposites.

Parameter Tested	Trial	Cu:Zn	Conc (M)	Time (hour)	pH	Leaf Extract (mL)	UV–Vis Intensity	Note
Cu:Zn ratio	1	1:1	0.1	1	10	20	0.91	
	2	1:2	0.1	1	10	20	1.05	best
	3	2:1	0.1	1	10	20	0.87	
Conc (M)	1	1:2	0.05	1	10	20	0.85	
	2	1:2	0.1	1	10	20	1.02	best
	3	1:2	0.15	1	10	20	0.92	
Time (h)	1	1:2	0.1	1	10	20	1.03	best
	2	1:2	0.1	2	10	20	0.97	
	3	1:2	0.1	3	10	20	0.91	
Ph	1	1:2	0.1	1	7	20	0.82	
	2	1:2	0.1	1	9	20	0.89	
	3	1:2	0.1	1	10	20	1.01	best
Leaf Extract (mL)	1	1:2	0.1	1	10	10	0.93	
	2	1:2	0.1	1	10	20	1.03	best
	3	1:2	0.1	1	10	30	0.98	

FTIR Analysis

Enset Leaf Extract

The proposed FTIR spectrum of the Enset leaf extract displays several characteristic bands associated with chemicals called phytochemicals active for the synthesis of NPs. A broader band observed approximately 3400 cm^{-1} is assigned to O–H stretching vibrations in phenols, alcohols, and flavonoids. The peak near 2920 cm^{-1} is comparable to C–H stretching vibrations of aliphatic compounds [29]. A band appearing around 1630 cm^{-1} is specified to C=O stretching or N–H bending, which suggests the existence of proteins or amide groups [30]. Peaks approximately 1050–1200 cm^{-1} correspond with C–O stretching vibrations of alcohols, phenols, and polysaccharides.

CuO/ZnO Nanocomposites

The broad absorption band observed in the FTIR spectra of ZnO NPs at 3400 cm^{-1} was attributed to the stretching vibrations of hydroxyl (–OH) groups and adsorbed water molecules. The H–O–H bending vibrations are for the peak at about 1600 cm^{-1}. In Figure 1, the absorption band at 545 cm^{-1} confirms the Zn–O stretching mode vibration, suggesting the successful formation of ZnO NPs, which is consistent with previously reported values around 550 cm^{-1} [31]. The Cu–O stretching is represented at 560 cm^{-1}, which is in relation to the value reported [32], confirming the formation of NPs. NCs have distinctive peaks in their FTIR spectra that belong to both ZnO and CuO. The presence of hydroxyl groups on the composite's surface is also shown in NCs by the broad band about 3400 cm^{-1} and the peak near 1600 cm^{-1}. Zn–O and Cu–O stretching vibrations are represented by bands at 500-550 cm^{-1} and 520–600 cm^{-1}, respectively [33], in the lower wavenumber range. These peaks' coexistence indicates the CuO/ZnO NCs' effective synthesis. Furthermore, minor changes in peak locations relative to individual metal oxides suggest that CuO and ZnO interact, and that phytochemicals from the Enset leaf extract help stabilize the structure of the NCs.

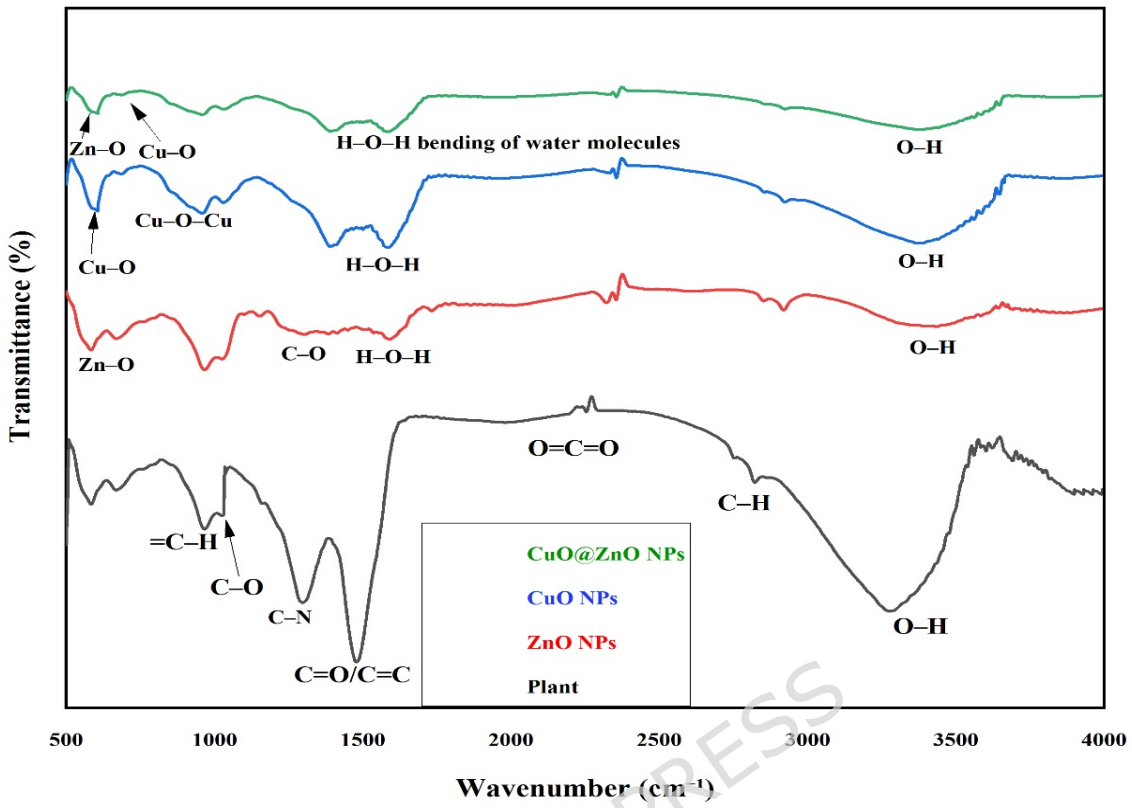

Figure 1: FTIR spectrum of synthesized CuO/ZnO NCs using Enset *(Ensete ventricosum)* leaf extract**,** confirming plant-derived functional groups and characteristic MO vibrations that indicate successful formation of the NCs.

XRD Analysis

The crystalline structures of the ZnO, CuO NPs, and the ZnO/CuO NCs synthesized using Enset leaf extract were investigated by the XRD analysis, as shown in Figure 2.

ZnO Nanoparticles

The XRD pattern exhibits prominent diffraction peaks at 2θ ≈ 31.8°, 34.4°, 36.3°, 47.5°, 56.6°, 62.8°, 67.9°, and 69.1°, corresponding to the crystallographic planes (100), (002), (101), (102), (110), (103), (112), and (201), respectively (Figure 2). These diffraction peaks are well indexed to the hexagonal wurtzite crystal structure of Zinc oxide (JCPDS card No. 36-1451)

[34, 35], confirming the high crystallinity and phase purity of the synthesized nanoparticles.

CuO Nanoparticles

CuO NPs exhibit significant diffraction peaks at 2θ ≈ 32.5°, 35.5°, 38.7°, 48.7°, 53.5°, 58.3°, 61.5°, and 66.2° according to their XRD pattern. These peaks correspond to the crystal planes (110), (−111), (111), (−202), (020), (−113), and (311), respectively, as shown in Figure 2. The monoclinic crystal structure of CuO (JCPDS card No. 48-1548) is consistent with these peaks [36, 37]. Phase-pure CuO NPs are produced, as no additional peaks are observed.

CuO/ZnO Nanocomposites

The effective synthesis of the composite structure is confirmed by the XRD pattern of the CuO/ZnO NCs, which shows diffraction peaks corresponding to both ZnO NPs and CuO NPs phases. The ZnO (100), (002), and (101) planes are represented by the large peaks at 31.8°, 34.4°, and 36.3°, while the CuO phase is responsible for the additional peaks at 35.5° and 38.7°, as shown in Figure 2.

These peaks' coexistence suggests that the nanocomposite contains both metal oxides. Furthermore, the relatively broad diffraction peaks suggest the nanoscale crystallite size of the synthesized materials. The calculated average crystallite size of the CuO/ZnO NCs was 24.5 nm, indicating successful formation of nanosized crystalline heterostructures [33]. Similar CuO/ZnO NCs synthesized via chemical routes have shown crystallite sizes in the range of 15–35 nm [38,39]. In addition to this present work demonstrates (24.5 nm), which is comparable to or slightly higher than values reported in previous studies (Table 5) [40] .

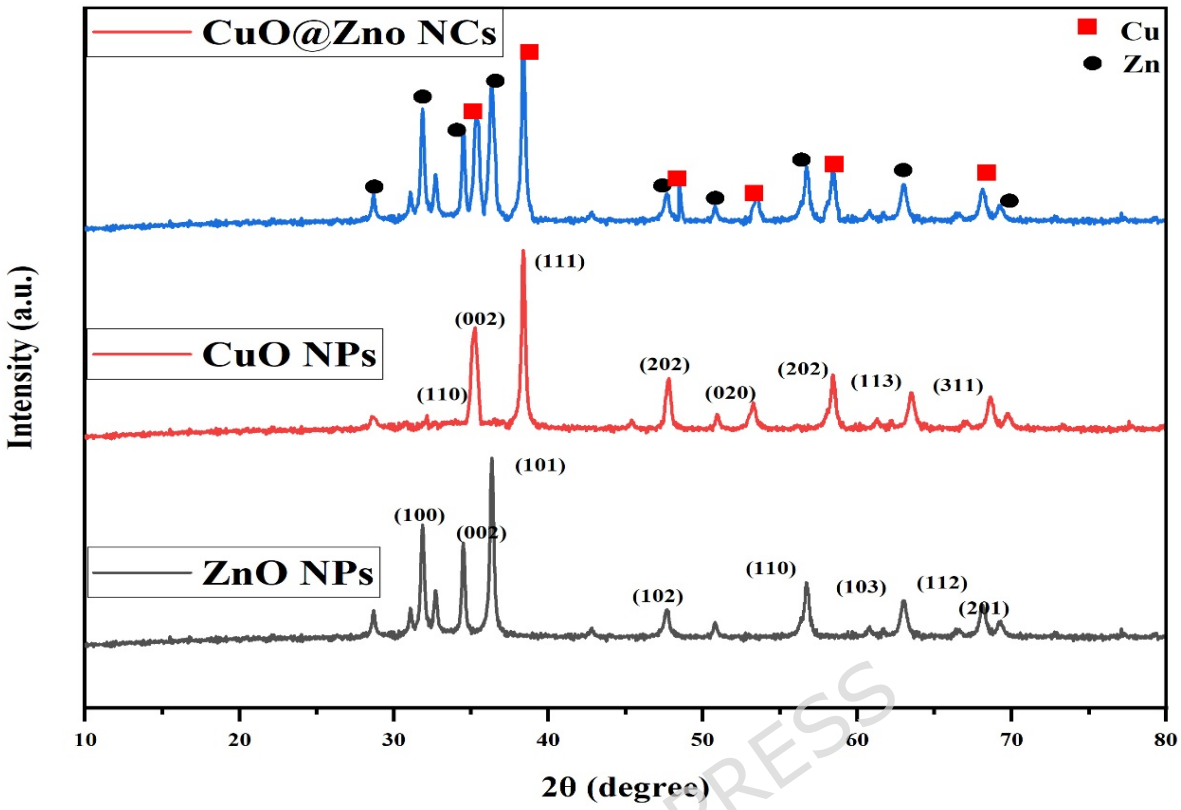

Figure 2: XRD pattern of biosynthesized CuO/ZnO nanocomposites using *Ensete ventricosum* leaf extract, confirming phase formation and crystallinity of the prepared material.

SEM Analysis

The surface morphological of ZnO, CuO, and CuO/ZnO nanocomposites prepared using Enset (*Ensete ventricosum*) leaf extract were examined using SEM. The SEM images were recorded at magnifications of 1500, 3000, and 1000. The images were recorded at relatively low magnification; therefore, the analysis is limited to general surface features rather than detailed nanostructure resolution.

According to the SEM images, ZnO-NPs showed that the surface morphologies are in the form of somewhat aggregated and nearly spherical distribution over the entire surface, as shown in Figure 3A. This is closely related to the reported literature [41].

The SEM images revealed that the average particle size was about 40 nm. The SEM micrographs of CuO NPs reveal slightly inconsistent, slightly aggregated particles with rough surfaces. The CuO NPs showed an average particle size of ~35 nm and were mainly distributed in flake-like morphologies. The significant surface roughness observed in Figures 3A and 3B suggests an increased surface area, which may enhance their catalytic and antibacterial performance. SEM images of CuO/ZnO NCs show that the CuO NPs have a uniform distribution on the ZnO particle surface, yielding a composite structure. The particles' heterogeneous morphology and clustered appearance indicate the NCs production. The CuO/ZnO NCs were found to possess an average particle size of approximately 45 nm, indicating successful heterostructure formation and slight particle growth compared to the individual metal oxide nanoparticles. Since XRD analyzes crystallite size while SEM measures total particle size, particle agglomeration may be the cause of the somewhat higher particle size shown in SEM compared to XRD data.

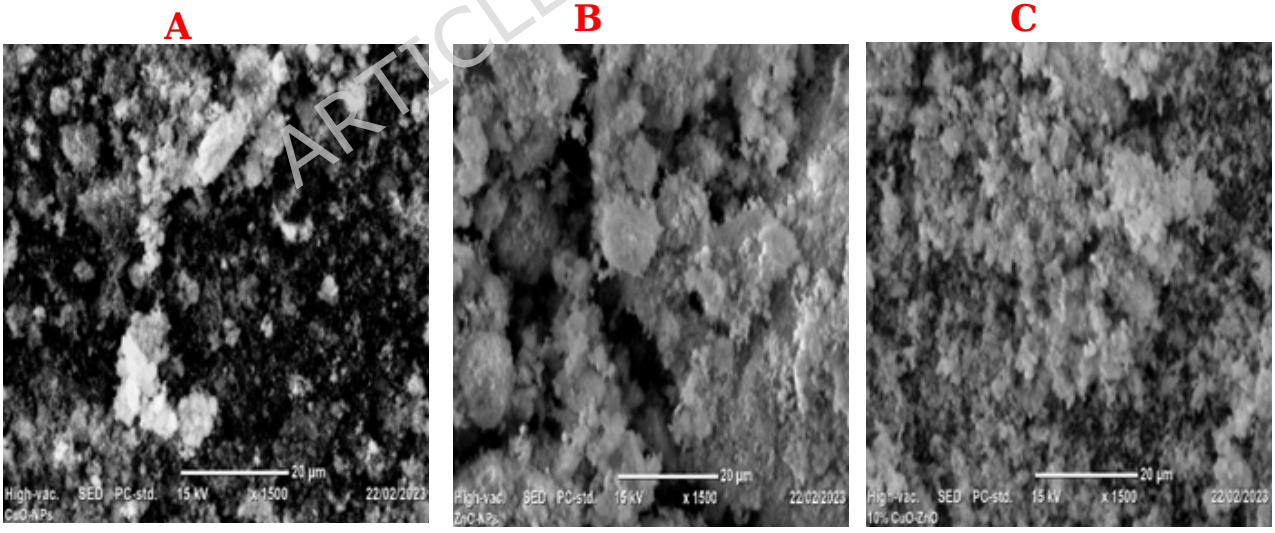

Figure 3: SEM images of biosynthesized nanomaterials showing (A) ZnO nanoparticles, (B) CuO nanoparticles, and (C) CuO/ZnO nanocomposites prepared using *Ensete ventricosum* leaf extract.

EDS Analysis

EDS was used for examining the elemental composition of the produced CuO/ZnO NCs. The EDS analysis further confirmed the successful formation of the CuO/ZnO composite, as the spectrum clearly displayed characteristic peaks corresponding to Cu, Zn, and O, indicating the purity and proper elemental composition of the synthesized nanocomposite. The existence of oxygen in the metal oxide structure is confirmed by the O Kα emission line, which is represented by a distinctive peak seen at about 0.52 keV (Figure 4)

Furthermore, the Cu Lα and Zn Lα emission lines are responsible for the significant peaks that arise at approximately 0.93 keV and 1.01 keV, respectively [42]. These peaks partially overlap, creating a comparatively large peak in the low-energy portion of the spectrum because of the extremely small energy difference between the Cu and Zn L-lines. This overlap is commonly observed in EDS spectra of Cu–Zn-based NCs because the detector resolution is typically insufficient to completely separate these closely spaced emission lines.

Moreover, the presence of Cu and Zn is further confirmed by additional peaks observed in the high-energy region of the EDS spectrum. The Cu Kα transition is represented by the peaks that emerge around 8.04 keV, and the Zn Kα transition is represented by the peaks that appear around 8.64 keV. The equivalent Kβ transitions of Cu and Zn are linked to minor peaks seen at slightly higher energy. The simultaneous appearance of both L- and K-series emission lines clearly confirms the coexistence of Cu and Zn elements in the synthesized material.

Importantly, no additional impurity peaks were detected in the spectrum, indicating the high purity of the obtained nanocomposite. These results confirm the successful formation of the CuO/ZnO nanostructured composite and the effective incorporation of both CuO and ZnO phases.

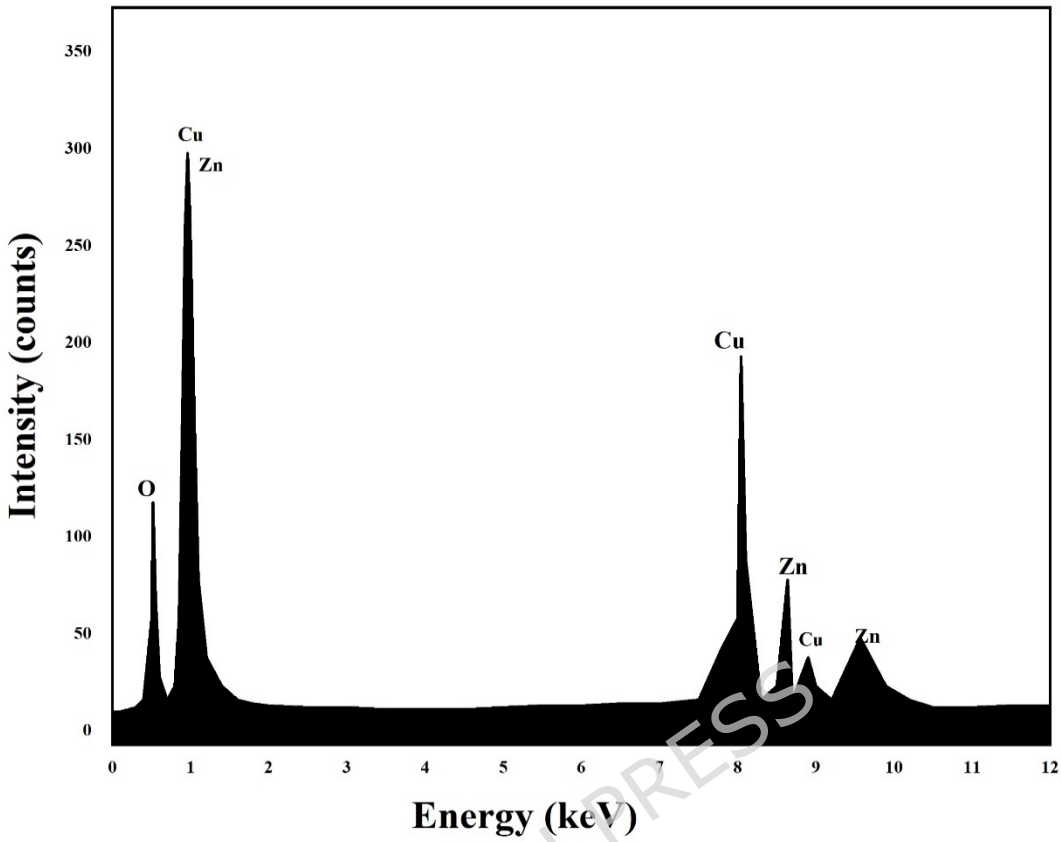

Figure 4: EDS spectrum of biosynthesized CuO/ZnO NCs using *Ensete ventricosum* leaf extract, indicating the elemental composition of the prepared material.

The approximate quantitative elemental composition obtained from EDS analysis is summarized below in Table 2:

Table 2: Elemental composition of CuO/ZnO nanocomposites obtained from EDS analysis.

Element	Weight (%)	Atomic (%)
Cu	~32–38	~18–22
Zn	~28–35	~15–20
O	~30–40	~60–65

The quantitative results further support the presence and proper distribution of Cu, Zn, and O elements in the nanocomposite, consistent with the formation of CuO/ZnO heterostructures.

Optical Properties (UV–Vis)

To evaluate the optical behavior of CuO, ZnO, and CuO/ZnO NCs, their UV–Visible absorption spectra were presented.

The band absorption of ZnO is indicated by a prominent peak at 354 nm for pure ZnO nanoparticles, which is in close agreement with Ref. [43], reported at 350 nm. Using the Tauc plot, the estimated optical energy of the band gap for ZnO was determined to be 3.28 eV, which is in close agreement with a recently published paper [44]. CuO NPs displayed an optical band gap of 1.55 eV and a wider absorption band that extended into the visible spectrum with a distinctive absorption edge at 570 nm. This absorption of visible light is explained by CuO narrow band gap.

In comparison to pure ZnO, the CuO/ZnO NCs showed a red shift toward longer wavelengths (~421 nm) as shown in Figure 5. The UV–Vis absorption peak at 421 nm indicates a red shift relative to many literature reports, suggesting enhanced visible light absorption due to the formation of a CuO/ZnO heterojunction (Table 5) [45].

The band gap energy of the CuO/ZnO nanocomposites was estimated using the Tauc plot by extrapolating the linear portion of the $(\alpha h\nu)^2$ versus $h\nu$ curve to the energy axis. The nanocomposite's calculated band gap energy was lowered to roughly 3.25 eV (Figure 6), indicating that a CuO–ZnO heterojunction had formed, which is consistent with the band gap reduction reported by Amnah Al-Yunus et al. in CuO–NiO nanocomposites synthesized [46]. Strong interfacial contact and efficient charge transfer between CuO and ZnO are responsible for the band gap narrowing. The CuO/ZnO NCs have

greater visible light absorption and decreased band gap, enabling better electron–hole separation, which is essential for the production of ROS and contributes to the observed increased antibacterial and antioxidant properties [47].

The presence of phytochemical compounds from *Ensete ventricosum* extract may also contribute to improved nanoparticle stability, dispersion, and surface reactivity, further enhancing the optical and biological performance of the nanocomposites.

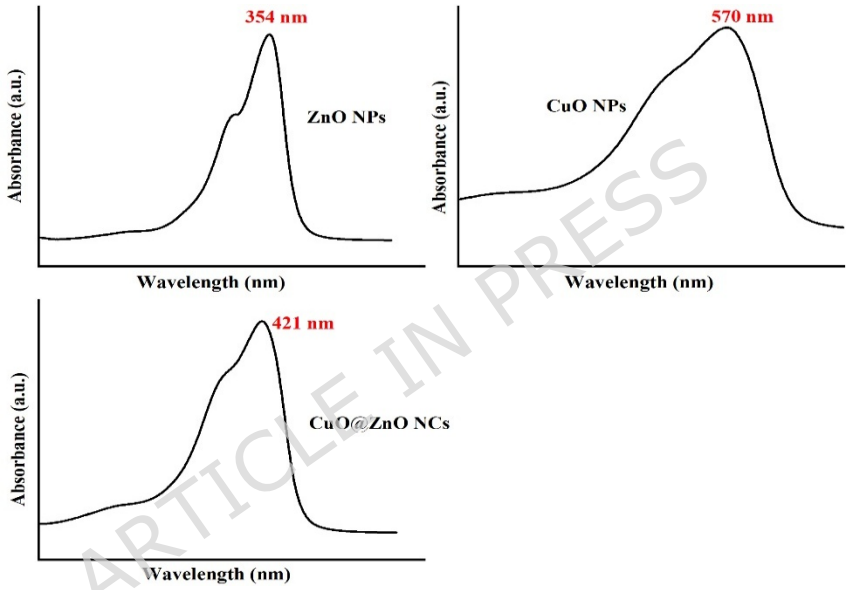

Figure 5: UV–Vis spectra of ZnO NPs, CuO NPs, and CuO/ZnO NCs synthesized using Enset (*Ensete ventricosum*) leaf extract, indicating the optical properties and successful formation of the NCs.

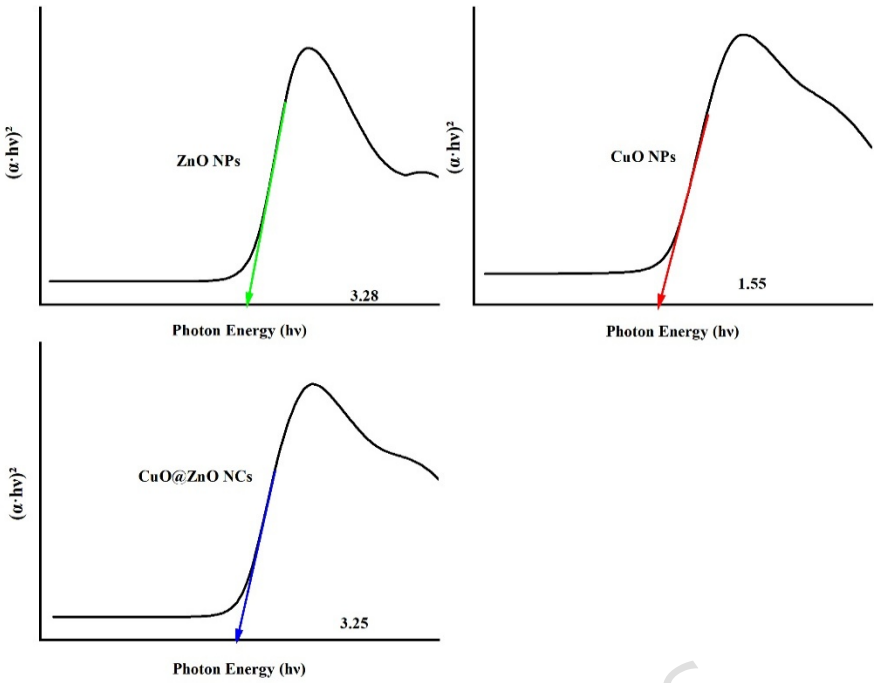

Figure 6: Tauc plot of $(\alpha h\nu)^2$ versus $h\nu$ of the CuO/ZnO NCs synthesized using Enset (*Ensete ventricosum*) leaf extract.

Antimicrobial Activity

The antibacterial efficacy of the synthesized ZnO, CuO, and CuO/ZnO NCs was systematically evaluated using the disk diffusion assay against Gram-positive *S. aureus* and Gram-negative *E. coli* to assess their broad-spectrum antimicrobial activity (Figure 7). The CuO/ZnO nanocomposites (NCs) produced the largest inhibition zones, ranging from 19 to 22.64 mm, indicating superior antibacterial efficiency against both tested bacterial strains.

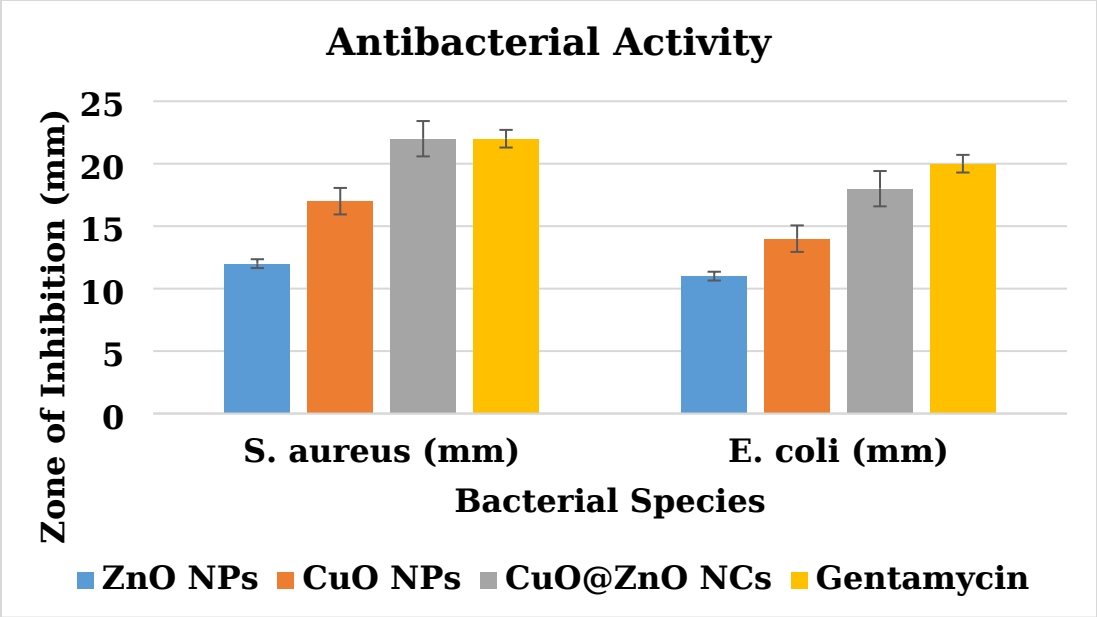

Figure 7: Comparative antibacterial activity of ZnO NPs, CuO NPs, and CuO/ZnO NCs synthesized using Enset (*Ensete ventricosum*) extract based on the measured zone of inhibition.

Table 3: Antibacterial activity of CuO/ZnO NCs evaluated by disk diffusion method and minimum inhibitory concentration (MIC) against *S. aureus* and *E. coli.* The results are expressed as mean inhibition zone diameter (mm ± SD, n = 3) and MIC values (µg/mL).

Sample	*S. aureus* (mm)	*E. coli* (mm)	MIC (*S. aureus*) µg/mL	MIC (*E. coli*) µg/mL
CuO/ZnO NCs	22.64 ± 0.30	19.21 ± 0.41	41	48

The disk diffusion results showed larger inhibition zones against Gram-positive Staphylococcus aureus (22.64 mm) compared to Gram-negative *E. coli* (19.21 mm) (Figure 7), which is consistent with the MIC results, where *S. aureus* exhibited a lower MIC value (41 µg/mL) than E. coli (48 µg/mL), indicating higher susceptibility of Gram-positive bacteria (Table 2). The

combined results from both methods indicate a consistent antibacterial trend, confirming higher susceptibility of Gram-positive bacteria. The thicker peptidoglycan layer in Gram-positive bacteria is more susceptible to nanoparticle-induced damage, whereas the outer membrane of Gram-negative bacteria provides an additional barrier

Furthermore, the antibacterial performance of the CuO/ZnO NCs was higher than that reported for Cu-doped ZnO NCs (16–18 mm) synthesized by Natsanet Woldesenbet Rayya *et al* [48], highlighting the enhanced efficacy of the present system. In addition, the synthesized NCs show superior inhibition zones, outperforming several previously reported materials (Table 5) [12]. This improvement can be attributed to several synergistic mechanisms. First, the formation of a heterojunction between CuO and ZnO facilitates efficient charge transfer, leading to enhanced generation of reactive oxygen species (ROS). These ROS induce oxidative stress in bacterial cells, resulting in damage to cellular components such as lipids, proteins, and DNA, ultimately causing cell death [49].

In addition, the relatively small particle size and high surface-to-volume ratio of the nanocomposites increase the contact area between the nanoparticles and bacterial membranes [50]. This promotes stronger interaction with the cell surface and facilitates easier penetration into the bacterial cell wall, leading to membrane disruption and leakage of intracellular contents [51]. The combined effects of ROS generation, membrane disruption, and structural susceptibility make the CuO/ZnO NCs highly effective antibacterial agents. One-way ANOVA revealed significant differences in antibacterial activity among the tested samples ($p < 0.05$).

Antibacterial Mechanism

The antibacterial activity of CuO/ZnO nanocomposites may be attributed to several mechanisms commonly reported for metal oxide nanomaterials [52].

These include the generation of reactive oxygen species (ROS), which can induce oxidative stress and damage cellular components, and the possible release of Cu^{2+} and Zn^{2+} ions, which may disrupt membrane integrity and inhibit essential enzymatic functions. In addition, the CuO–ZnO heterojunction may enhance charge separation, potentially increasing ROS production, while direct contact between nanoparticles and bacterial cells may further contribute to membrane damage. However, these mechanisms are proposed based on previous literature and were not directly investigated in this study; therefore, the antibacterial effect is likely due to combined physicochemical interactions [53-55].

Antioxidant Assay

The antioxidant activity of CuO, ZnO, and CuO/ZnO NCs was assessed by using the DPPH. A dose-dependent antioxidant response was indicated by the gradual increase in scavenging activity with increasing concentration (25–200 µg/mL) as shown in Table 4.

Table 4: DPPH radical scavenging activity of CuO/ZnO NCs at different concentrations

Concentration (µg/mL)	Mean % Inhibition ± SD (n = 3)
25	18.33 ± 0.58
50	27.67 ± 0.58
75	32.17 ± 0.76
100	47.53 ± 0.50
125	56.13 ± 0.23
150	65.93 ± 0.90
175	71.77 ± 0.25
200	80.53 ± 0.50

Values are expressed as mean ± SD (n = 3). Different superscript letters indicate statistically significant differences among concentrations according to one-way ANOVA ($p < 0.05$).

The DPPH radical scavenging activity of the CuO/ZnO nanocomposites increased progressively with increasing concentration, reaching a maximum inhibition of 80.53 ± 0.50% at 200 µg/mL. Statistical analysis using one-way ANOVA revealed significant differences among the tested concentrations ($p < 0.05$), confirming the concentration-dependent antioxidant activity of the synthesized nanocomposites. The IC_{50} value was calculated using linear interpolation between the two nearest concentrations surrounding 50% inhibition between 100 µg/mL and 125 µg/mL as shown in Equation 4.

$$IC_{50} = C_1 + \frac{(50 - I1)}{(I2 - I1)} \times (C2 - C1) \quad \text{.....Equation 4}$$

$$IC_{50} = 100 + \frac{(50 - 47.53)}{(56.13 - 47.53)} \times (125 - 100)$$

$$IC_{50} = 107.18 \text{ µg/mL}$$

The IC_{50} value of the CuO/ZnO NCs was determined to be 107.18 µg/mL using linear interpolation between concentrations exhibiting 47.53% and 56.13% inhibition (Figure 8).

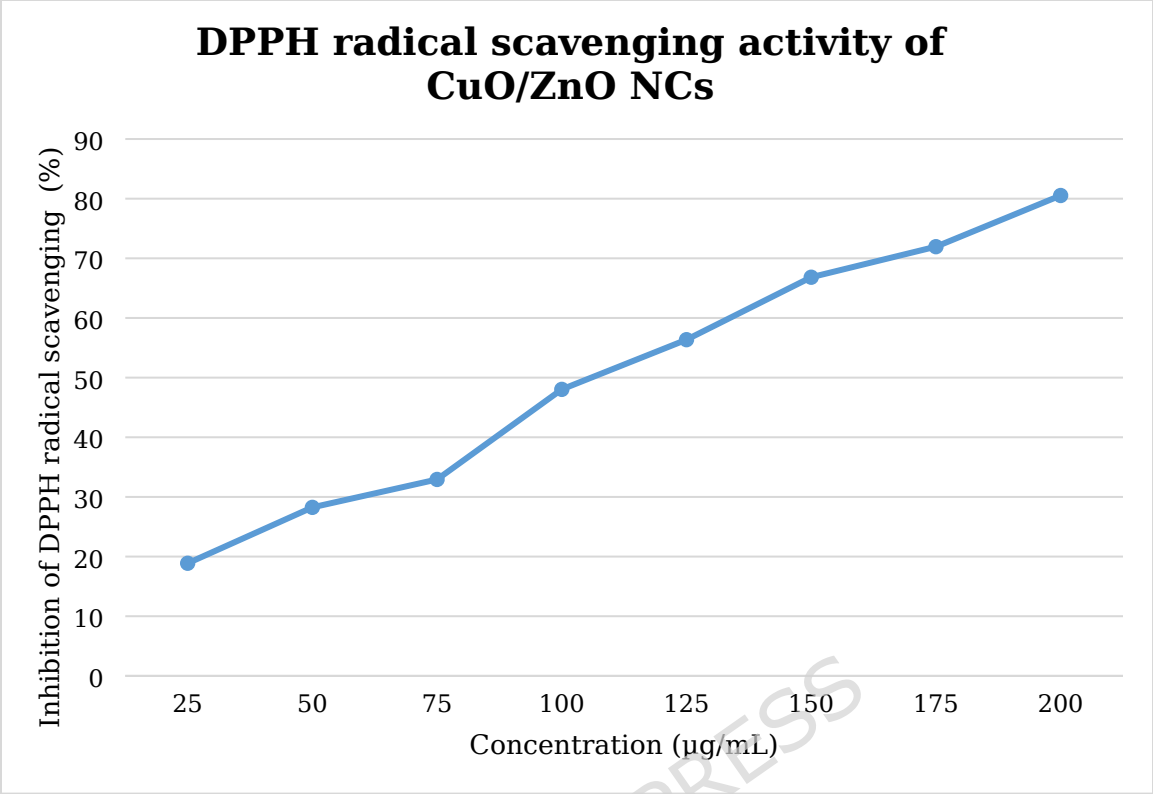

Figure 8: DPPH radical scavenging activity of CuO/ZnO NCs at different concentrations (mean ± SD, n = 3). The results demonstrate a concentration-dependent increase in radical scavenging activity. The IC_{50} value was estimated to be 107.18 µg/mL.

The CuO/ZnO NCs have the lowest IC_{50} (≈107.18 µg/mL) compared with CuO NPs (≈150.21 µg/mL) and ZnO NPs (≈179.95 µg/mL), indicating their higher radical scavenging activity (Figure 9), which was due to: functional groups of surface phytochemicals, concentration-dependent behavior, and context-dependent redox behavior. Bioactive phytochemicals are present on the surface of NCs through the application of Enset leaf extract during green synthesis.

In terms of the antioxidant activity (IC_{50} = 107.18 µg/mL), the synthesized NCs show strong free radical scavenging ability, which is comparable to or

slightly lower than some chemically synthesized counterparts but remains significant considering the environmentally friendly synthesis route (Table 5).

By donating hydrogen or electrons, these functional groups act as a factor for neutralization of DPPH radicals [56]. Scavenging efficiency is increased by the electron-rich interface, which encourages effective electron donation to DPPH radicals. One-way ANOVA showed significant differences in antioxidant activity among the tested samples ($p < 0.05$).

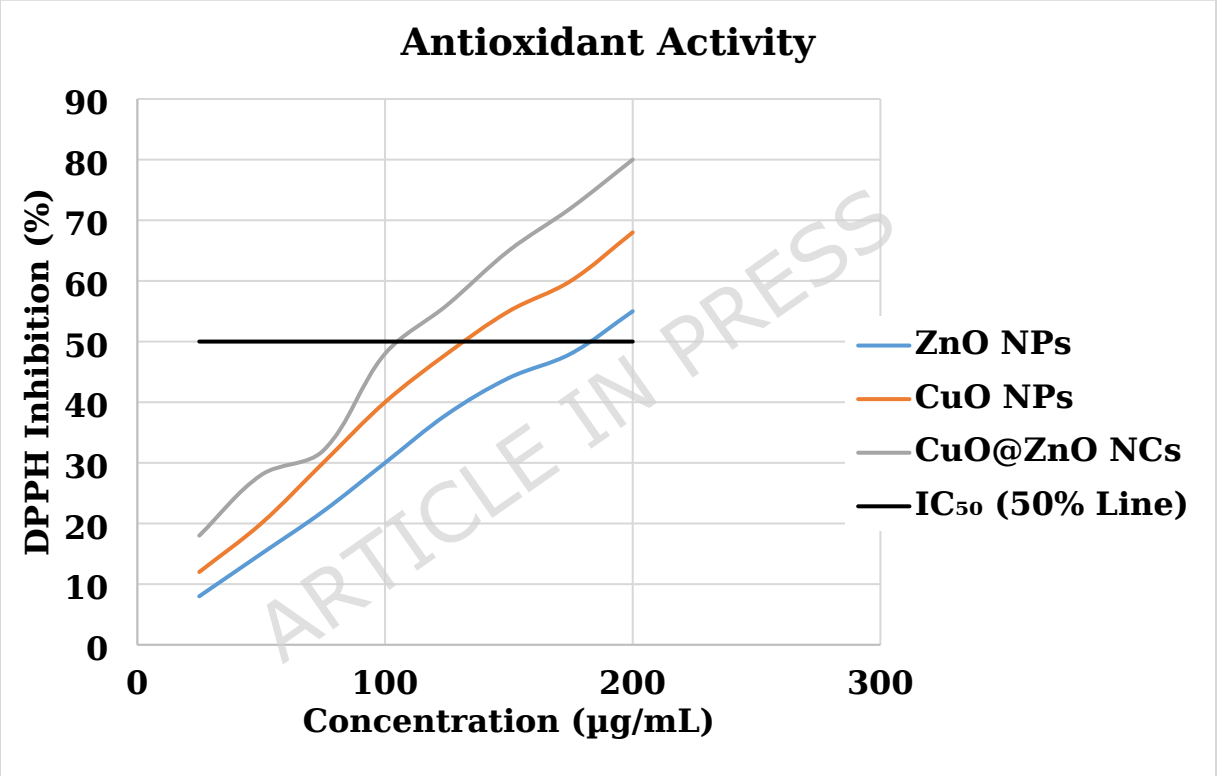

Figure 9: DPPH radical scavenging activity (%) of ZnO, CuO, and CuO/ZnO NCs at different concentrations.

To better evaluate the effectiveness of the synthesized nanocomposites, a comparative analysis with previously reported studies is essential. Table 5 summarizes the structural, optical, antibacterial, and antioxidant properties of CuO/ZnO nanocomposites reported in the literature alongside the present work.

Table 5: Comparison of structural, optical, antibacterial, and antioxidant properties of CuO/ZnO nanocomposites with literature reports

Study	Synthesis Method	UV–Vis Absorption (nm)	Crystallite Size (nm)	Antibacterial Activity (mm) (*S. aureus*/*E. coli*)	IC_{50} (µg/mL)	Key Remarks	
This work	Green synthesis	421	24.5	22.64/19.21	107	Enhanced antibacterial and antioxidant activity due to CuO/ZnO heterojunction	
Negash et al., 2021	Sol–gel synthesis	~380–420	16–30	18–24 / 15–22	Not reported	Strong antibacterial activity due to ROS generation and CuO/ZnO synergy	[57]
Tariq et al (2019) Microbial Pathogenesis	Co-precipitation method	~370–410	20–35	16-23 / 14–20	Not reported	Improved antibacterial performance compared to pure CuO and ZnO due to structural defects	[38]
Madara et al (2024) Scientific Reports	Hydrothermal synthesis	~400–430	15–28	20–26 / 18–24	Not reported	Surface modification enhances antibacterial activity and stability	[39]
Ahmed Nafia et al (2026) Scientific Reports	green synthesis	~405–420	18–32	21–27 / 17–23	Not reported	Strong activity against MDR bacteria due to heterojunction-induced ROS production	[58]
Ali et al. 2024) Heliyon	Chemical/combustion	~380–400	~24.9	~15–18 / ~14–16	~85–95	Comparable crystallite size;	[40]

						slightly stronger antioxidant activity	
Zhang et al. (2025) MDPI Catalysts	Green synthesis	~358	5–45	Strong (qualitative)	Not reported	A smaller band gap improves photocatalytic activity	[21]

Table 5 compares the structural, optical, antibacterial, and antioxidant properties of the synthesized CuO/ZnO nanocomposites with those reported in previous studies.

Overall, the results confirm that the green synthesis strategy not only provides an eco-friendly alternative but also yields CuO/ZnO nanocomposites with competitive or enhanced structural and functional properties, making them promising candidates for biomedical and environmental applications.

Structure Property Relationship

The produced CuO/ZnO NCs, which improved antioxidant and antibacterial properties, are closely linked to their structural features. A comparatively tiny crystallite size was found by XRD examination, which raises the surface area and surface-to-volume ratio [59]. The CuO–ZnO heterojunction interface and surface functionalization from Enset leaf phytochemicals improve the NCs functional qualities. The reported biological activities are largely determined by these combined structural properties.

The number of active surface sites accessible for interaction is greatly increased by the smaller crystallite size. By increasing interaction between NPs and bacterial cells, a larger surface-to-volume ratio promotes membrane breakdown and increases antibacterial efficiency [60]. In antioxidant tests, the larger surface area simultaneously allows for more interaction with free radicals. As a result, both ROS-mediated antibacterial activity and electron transfer-based antioxidant performance are improved in the NCs system [61].

During green synthesis, the Enset leaf extract serves a number of essential functions. It serves as a size-controlling agent that controls crystal growth, a stabilizing (capping) agent that inhibits particle aggregation, and a reducing agent during nanoparticle formation. Functional groups like hydroxyl and carbonyl groups are added to the surface of the NPs by the phytochemicals in the extract [62]. By promoting electron donation and stabilizing reactive species, these surface-bound biomolecules improve the material's capacity to scavenge radicals and hence greatly increase its antioxidant efficacy [63]. Additionally, a heterojunction formed by the CuO–ZnO contact enhances charge separation inside the composite structure. This heterostructure increases the production of reactive oxygen species while decreasing electron-hole recombination. By causing oxidative stress in microbial cells, the increased generation of ROS enhances antibacterial activity [58, 59]. Therefore, the formation of the CuO–ZnO heterojunction establishes a direct link between structural engineering and enhanced biological activity, demonstrating a clear structure–property relationship in the synthesized NCs [66].

Conclusion

In this study, *Ensete ventricosum* (Enset) leaf extract was successfully used as a natural reducing and stabilizing agent for the green synthesis of CuO/ZnO binary metal oxide nanocomposites in an eco-friendly and sustainable manner. The phytochemical-assisted synthesis enabled controlled nucleation and growth, producing well-crystallized nanostructures with uniform distribution. Structural and optical analyses (XRD, FTIR, SEM, and UV–Vis) confirmed the formation of a CuO/ZnO heterojunction and effective surface functionalization by plant-derived biomolecules.

The CuO/ZnO nanocomposites exhibited significantly enhanced antibacterial activity compared to individual oxides, with inhibition zones of 22.64 mm against Gram-positive Staphylococcus aureus and 19.21 mm against Gram-

negative Escherichia coli. This improvement is attributed to synergistic effects, including reactive oxygen species (ROS) generation, efficient charge separation at the CuO/ZnO interface, and enhanced membrane interactions.

In addition, antioxidant evaluation using the DPPH assay showed IC_{50} values of approximately 180 µg/mL (ZnO NPs), 150 µg/mL (CuO NPs), and 107.18 µg/mL for CuO/ZnO nanocomposites, confirming superior antioxidant performance of the composite. The structure–property relationship suggests that reduced crystallite size, high surface area, phytochemical capping, and heterojunction formation collectively govern the enhanced biological activity.

Overall, this work demonstrates a scalable, cost-effective, and environmentally friendly approach for producing multifunctional CuO/ZnO nanocomposites with improved antibacterial and antioxidant properties. The findings provide a strong foundation for the development of sustainable nanomaterials for environmental remediation and biomedical applications.

Funding

This research did not receive any specific grant from funding agencies in the public, commercial, or not-for-profit sectors.

Conflicts of Interest

The authors declare that they have no competing interests.

Data Availability

The datasets generated and/or analyzed during the current study are available from the corresponding author on reasonable request.

References

1. Justyna Ł, Magdalena W, Bartosz K, Maria T, Julia K. Disinfectant-induced bacterial resistance and antibiotic

cross-resistance mechanisms and clinical relevance. *Clin. Exp. Med.,* **26***, 26* (2026). https://doi.org/10.1007/s10238-025-01950-2.

2. Chandimali N, Bak SG, Park EH, Lim H, Won Y, Kim E. Free radicals and their impact on health and antioxidant defenses: a review. *Cell Death Discov*. **11**, 19 (2025). https://doi:10.1038/s41420-024-02278-8.
3. Nwobodo DC, et al. Antibiotic resistance: The challenges and some emerging strategies for tackling a global menace. *J. Clin. Lab. Anal*. **36**, e24655 (2022). https://doi.org/10.1002/jcla.24655.
4. Medic BS, Tomic N, Lagopati N, Gazouli M. Advances in metal and metal oxide nanomaterials for topical antimicrobial applications: insights and future perspectives. *Molecules*, **29**, 5551 (2024). https://doi.org/10.3390/molecules29235551.
5. Martin C, Nourian A, Babaie M, Nasr GG. Environmental, health and safety assessment of nanoparticle application in drilling mud: Review. *Geoenergy Science and Engineering*. **226**, 211767 (2023). https://doi:10.1016/j.geoen.2023.211767.
6. Osman AI, Zhang Y, Farghali M, Rashwan AK, Eltaweil AS. Synthesis of green nanoparticles for energy, biomedical, environmental, agricultural, and food applications: A review. *Environ. Chem. Lett***. 22**, 841–887 (2024). https://doi.org/10.1007/s10311-023-01682-3
7. Muanenda M, Mengesha W. Harnessing the medicinal potential of Enset (Ensete ventricosum) in Ethiopian traditional medicine: A synthesis of current knowledge. *Food Sci. Nutr.* **13**, 1-11 (2025). https://doi:10.1002/fsn3.71169.
8. Woredas E, Zone G, Jarso A, Demissew S, Wondimu T. Morphological diversity and ethnobotanical study of Enset (*Ensete ventricosum*) (Welw.) Cheesman in Kebena, Cheha. *Plant Sci. Today* **11(4),** 135–142 (2023). https://doi:10.11648/j.plant.20231104.14.
9. Lung I, Stegarescu A. Biosynthesis of nanoparticles using plant extracts and essential oils. *Molecules* **28**, 3060 (2023). https://doi.org/10.3390/molecules28073060.

10. Hanna DH, et al. Plant-derived nanoparticles: Green synthesis, factors, and bioactivities. *Next Materials* **9,** 101275 (2025). https://doi:10.1016/j.nxmate.2025.101275.
11. Irradiation L, et al. Optimization of Facile Synthesized ZnO/CuO Nanophotocatalyst for Organic Dye Degradation by Visible Light Irradiation Using Response Surface Methodology. *Catalysts* **11**, 1509 (2021). https://doi.org/10.3390/catal11121509.
12. Bekele S, Goddati M, Lee J, Gochole F, Teshome L, Kedir F. ZnO/CuO nanocomposites for enhanced photocatalytic and antibacterial applications: A comparative study of synthesis methods. *J Sci. Adv. Mater. Devices* **10**, 100898 (2025). https://doi:10.1016/j.jsamd.2025.100898.
13. Robi ZH, Nemera DJ, Gebremichael TE, Muleta GG. Dual-functional nitrogen-doped carbon dot/copper oxide nanocomposites for electrochemical sensing of ascorbic acid and antimicrobial applications. *BMC Chem*. **19**, 298 (2025). https://doi:10.1186/s13065-025-01639-3.
14. El Sawaf AK, El Moslamy SH, Kamoun EA, Hossain K. Green synthesis of trimetallic CuO/Ag/ZnO nanocomposite using plant extract: characterization, statistically experimental designs, and antimicrobial assessment. *Sci. Rep*. **14,** 67579 (2024). https://doi:10.1038/s41598-024-67579-5.
15. Pawar AA, et al. Azadirachta indica-Derived silver nanoparticle synthesis and its antimicrobial applications. *Int. J. Biomater*. **2022**, 4251229 (2022). https://doi:10.1155/2022/4251229.
16. Swain M, Mishra D, Sahoo G. A review on green synthesis of ZnO nanoparticles. *Discover Appl. Sci.* 7, 997 (2025). https://doi:10.1007/s42452-025-06957-8.
17. Boddu S, et al. Green synthesis of copper oxide nanoparticles (CuONPs) using Ricinus communis: efficient photocatalytic dye

degradation and antibacterial applications. Water *Air Soil Pollut*. **236**, 209 (2025). https://doi:10.1007/s11270-025-07841-2.

18. Siddiqui VU, Ansari A, Chauhan R, Siddiqi WA. Green synthesis of copper oxide (CuO) nanoparticles by Punica granatum peel extract. Mater. *Today Proc*. **36**, 751–755 (2021). https://doi:10.1016/j.matpr.2020.05.504.
19. Zhou X-Q, et al. Zinc oxide nanoparticles: synthesis, characterization, modification, and applications in food and agriculture. *Processes*. 11, 1193 (2023). https://doi:10.3390/pr11041193.
20. Jaishi DR, et al. Plant-mediated synthesis of zinc oxide (ZnO) nanoparticles using Alnus nepalensis D. Don for biological applications. *Heliyon* 10, e39255 (2024). https://doi:10.1016/j.heliyon.2024.e39255.
21. Yu J, Zhuang S, Xu X, Zhu W, Feng B, Hu J. Photogenerated electron reservoir in hetero-p-n CuO-ZnO nanocomposite device for visible-light-driven photocatalytic reduction of aqueous Cr(VI). *J. Mater. Chem*. A **3**, 1199 (2015). https://doi.org/10.1039/C4TA05514K
22. BaQais A, Alam MW, Farhan M, Muteeb G, Allag N, Mushtaq S. Probe-sonicated synthesis of CuO–ZnO hybrid nanocomposite for photocatalytic and supercapacitor applications. *Inorganics* **11**, 370 (2023). https://doi:10.3390/inorganics11090370.
23. Gebremichael TE, Tesfaye E, Abebe T, Bekele A, Robi ZH, Gebremikael TE. Bio-derived NiO nanoparticles from Colocasia esculenta leaf extract with enhanced antibacterial activity and efficient photocatalytic degradation of methylene blue. *RSC Adv*. **16,** 2030–2043 (2026). https://doi:10.1039/D5RA08840B.
24. Joudeh N, Linke D. Nanoparticle classification, physicochemical properties, characterization, and applications: a comprehensive review for biologists. *J. Nanobiotechnol.* **20**, 262 (2022). https://doi:10.1186/s12951-022-01477-8.

25. Flores-Rábago KM, Rivera-Mendoza D, Vilchis-Nestor AR, Juarez-Moreno K, Castro-Longoria E. Antibacterial activity of biosynthesized copper oxide nanoparticles (CuONPs) using Ganoderma sessile. *Antibiotics* **12,** 1251 (2023). https://doi:10.3390/antibiotics12081251.

26. Ghodake VS, Koyale PA. Exploring the antibacterial properties of ZnO nanorods–CuO nanoflowers: a mode of action approach. *RSC Adv*. **15**, 32995 (2025). https://doi:10.1039/d5ra04095g.

27. Bedlovičová Z, Strapáč I, Baláž M, Salayová A. A brief overview on antioxidant activity determination of silver nanoparticles. *Molecules* **25,** 3143 (2020) https://doi:10.3390/molecules25143191.

28. Salari S, Esmaeilzadeh Bahabadi S, Samzadeh-Kermani A, Yosefzaei F. In-vitro evaluation of antioxidant and antibacterial potential of green-synthesized silver nanoparticles using Prosopis farcta fruit extract. Iran *J. Pharm. Res*. **18,** 430–455 (2019).

29. Dai F, Zhuang Q, Huang G, Deng H, Zhang X. Infrared spectrum characteristics and quantification of OH groups in coal. *ACS Omega* **8**, 17064–17076, (2023). https://doi:10.1021/acsomega.3c01336.

30. Metwally AM, Aly SAA, Makled SO, Abdelkader AMS. Biosorption of methylene blue from industrial wastewater using silicon dioxide nanoparticles and Cladophora glomerata. *Alexandria Eng. J.* **130**, 115–138 (2025). https://doi:10.1016/j.aej.2025.09.004.

31. Paul P, et al. Crystallographic facet engineering of ZnO nanoparticles for photocatalytic organic pollutant degradation and antibacterial activity. Mater. Adv. **6,** 4696–4704 (2025). https://doi:10.1039/d5ma00316d.

32. Said MI, Othman AA, Abd EM. Mesoporous CuO nanoparticles with tunable size and different morphologies. *RSC Adv*. **11**, 37801–37813 (2021). https://doi.org/:10.1039/d1ra04780a.

33. Jeevarathinam M, Asharani IV. Synthesis of CuO, ZnO nanoparticles, and CuO-ZnO nanocomposite for enhanced

photocatalytic degradation of Rhodamine B: a comparative study. *Sci. Rep*. **14**, 9718 (2024). https://doi:10.1038/s41598-024-60008-7.

34. Ramesh S, et al. Nanorod-like structure of ZnO nanoparticles and Zn_8O_8 clusters using 4-dimethylamino benzaldehyde to study physicochemical and antimicrobial properties. *Nanomater*. **13**, 166 (2022). https://doi:10.3390/nano13010166.
35. Bhushan M, Jha R, Bhardwaj R, Sharma R. Serrated hexagonal ZnO nanoparticles: synthesis and characterization. *Mater. Today Proc*. **48**, 629–632 (2022). https://doi:10.1016/j.matpr.2021.05.686.
36. Kumar MSS, Harini HV, Nagaraju G, Nirmala B. Combustion synthesis CuO nanoparticles: application to photocatalytic activity. *Mater. Today Proc*. **49**, 860–864 (2022). https://doi:10.1016/j.matpr.2021.06.043.
37. Mwafy EA, Mousa SM, El-Bassyouni GT. Catalytic degradation of 4-nitrophenol using CuO nanoparticles: structural, optical and catalytic properties. *Plasmonics* **20,** 10273–10285 (2025). https://doi:10.1007/s11468-025-03007-2.
38. Jan T, Azmat S, Mansoor Q, Waqas HM, Adil M, Ilyas SZ, Ahmad I, Ismail M. Superior antibacterial activity of ZnO–CuO nanocomposite synthesized by a chemical co-precipitation approach. *Microb. Pathog*. 134, 103579 (2019). https://doi.org/10.1016/j.micpath.2019.103579.
39. Jayanetti, M.; Thambiliyagodage, C.; Liyanaarachchi, H.; Ekanayake, G.; Mendis, A.; Usgodaarachchi, L. In vitro influence of PEG functionalized ZnO-CuO nanocomposites on bacterial growth. *Sci. Rep*. **14**, 1293 (2024). https://doi.org/10.1038/s41598-024-52014-6.
40. Aziz, S.N.; Abdulwahab, A.M.; Aldeen, T.S.; Alqabili, D.M.A. Synthesis, characterization, and evaluation of antibacterial and antifungal activities of CuO-ZnO-Co3O4 nanocomposites. *Heliyon* **11,** 10 (2024). https://doi.org/10.1016/j.heliyon.2024.e37802.

41. Raha S, Ahmaruzzaman M. ZnO nanostructured materials and their potential applications: progress, challenges and perspectives. *Nanoscale Adv.* **4**, 1868–1925 (2022). https://doi:10.1039/d1na00880c.
42. Szabó ÁI, Hasan R. Synergistic effects of CuO and ZnO nanoadditives on friction and wear in automotive base oil. *Appl. Sci*. **15**, 8258 (2025). https://doi:10.3390/app15158258.
43. Almoneef MM, et al. Exploring the multi-faceted potential: synthesized ZnO nanostructure characterization, photocatalysis, and crucial biomedical applications. *Heliyon* **10,** e32714 (2024). https://doi:10.1016/j.heliyon.2024.e32714.
44. Aksoy Pehlivanoglu S, Polat O. Exploring the structural and optical properties of Ir-doped ZnO thin films. *Opt. Mater.* **143**, 114179 (2023). https://doi:10.1016/j.optmat.2023.114179.
45. Fouda, A. et al. Photocatalytic Activity of Green-Synthesized Semiconductor CuO/ZnO Nanocomposites Against Organic Dye: An Assessment of Antimicrobial and Cytotoxicity Investigations. *Catalysts.* **15**, 1096 (2025).
46. Al-Yunus A. et al. Effect of synthesis conditions on CuO-NiO nanocomposites synthesized via saponin-green/microwave assisted-hydrothermal method. *Nanomaterials*. **14,** 308 (2024). https://doi:10.3390/nano14030308.
47. Karrari S, Mohammadzadeh H, Jafari R. Characterization of ZnO-CuO and ZnO-CuO-NiO nanocomposites prepared by co-precipitation and antibacterial properties. *Appl. Phys. A.* 131(2):147, 2025; doi:10.1007/s00339-025-08273-9.
48. Rayya NW, Etefa KT, Yimer AA, Muleta GG, Beyene TT. Green synthesis of Cu-doped ZnO nanocomposites using Phytolacca dodecandra root extract: improved photocatalytic and antibacterial activity and extended avocado shelf-life. *Sci. Rep*. **16**, 225 (2025). https://doi:10.1038/s41598-025-31793-6.

49. Gebretsadik A, Reddy SG, Gonfa BA, Abebe B. Ag-decorated Cu-doped ZnO nanomaterial for enhanced antibacterial application. *Sci. Rep.* **16**, 5552 (2026). https://doi:10.1038/s41598-026-35838-2.

50. Khosrovan S, Vahdati Khaki J, Mirjalili M, Matin MM, Esfandiari N. Synergistic mechanisms underlying optical, antimicrobial, anticancer, and antioxidant activities of multifunctional bioactive ZnO/CuO/clay nanocomposites. *ACS Appl. Bio Mater*. **8**, 11190–11205 (2025). https://doi:10.1021/acsabm.5c01884.

51. Gebremichael TE, Muleta GG, Tadele KT. Green synthesis of Ag-doped CuO nanocomposites using honey solution for evaluation of their antimicrobial and antioxidant activities. *Current Nanomaterials* **10**, 333-345 (2025). https://doi:10.2174/0124054615284528240201105900.

52. Alfei S, Schito GC, Schito AM, Zuccari G. Reactive oxygen species (ROS)-mediated antibacterial oxidative therapies: available methods to generate ROS and a novel option proposal. *Int. J. Mol. Sci.* **25**, 7182 (2024). https://doi:10.3390/ijms25137182.

53. Ma X, Zhou S, Xu X, Du Q. Copper-containing nanoparticles: mechanism of antimicrobial effect and application in dentistry: a narrative review. *Front. Surg.* **9**, 905892 (2022). https://doi:10.3389/fsurg.2022.905892.

54. Olajesu MO, Abegunde SM. Ecofriendly synthesis and characterization of CuO nanoparticles from Blighia sapida pods for antimicrobial applications. *Discover Chem* **3**, 40 (2026). https://doi:10.1007/s44371-026-00501-2.

55. El-Sherbiny GM, Shehata ME, Kalaba MH. Biogenic copper and copper oxide nanoparticles to combat multidrug-resistant Staphylococcus aureus: green synthesis, mechanisms, resistance, and future perspectives. *Biotechnol. Rep*. **46**, e00896, (2025). https://doi:10.1016/j.btre.2025.e00896.

56. Dhanaraj FI, Kalimuthu JK, Balamurugan PS, Subramani P, Katerere DR, Gurusamy M. Investigating the phytochemical profile and antioxidant activity of different solvent extracts of Sesamum prostratum Retz. *Plants* **14**, 40519 (2025). https://doi:10.3390/plants14040519.

57. Negash, Y.; Tolosa, B.; Bantewesen, T.; Bekele, G.; Feyisa, G. Antibacterial Activities of the CuO/ZnO Nanocomposite Grown on Silica Extracted from Bagasse Ash. *Ethiop. J. Sci. Sustain. Dev*. **8**, 1 (2021). https://doi.org/10.20372/ejssdastu:v8.i1.2021.319.

58. Obaid, A.N.; Abdelghany, T.M.; Soliman, A.M.; Mahmoud, N.N.; Mekky, A.E. Green mycosynthesis of a CuO/ZnO heterojunction nanocomposite using Aspergillus terreus and its antibacterial and anti-virulence activity against multidrug-resistant Escherichia coli. *Sci. Rep*. **16**, 12350 (2026). https://doi.org/10.1038/s41598-026-44775-z.

59. Jannat MR, et al. Validity of crystallite size determination methods based on XRD peak broadening in pure and metal-doped nickel ferrites. Results Mater. **28**, 100762 (2025). https://doi:10.1016/j.rinma.2025.100762.

60. Ozdal M, Gurkok S. Recent advances in nanoparticles as antibacterial agents. *ADMET DMPK* **10,** 115–129 (2022). https://doi:10.5599/admet.1172.

61. Dai Y, et al. Reactive oxygen species-scavenging nanomaterials for prevention and treatment of age-related diseases. J. Nanobiotechnol. **22**, 252 (2024). https://doi:10.1186/s12951-024-02501-9.

62. Elias EM, Meganathan G, Pappuswamy M. Green synthesis, characterization, and biological applications of silver nanoparticles from Pachira glabra leaf extract. *Microbe* 7**,** 100413 (2025). https://doi:10.1016/j.microb.2025.100413.

63. El-Seedi HR, et al. Updated review of metal nanoparticles fabricated by green chemistry using natural extracts: biosynthesis,

mechanisms, and applications. *Bioengineering* **11**, 1095 (2024). https://doi:10.3390/bioengineering11111095.

64. Dong S, et al. Ternary heterostructure-driven photoinduced electron-hole separation enhanced oxidative stress for triple-negative breast cancer therapy. J. *Nanobiotechnol*. **22**, 240 (2024). https://doi:10.1186/s12951-024-02530-4.

65. Wang G, et al. Engineered heterojunction microneedles initiate ROS-mediated ‘two-hit’ mechanism for accelerating impaired wound healing in diabetes. *Cell Biomater*. 100248 (2025). https://doi:10.1016/j.celbio.2025.100248.

66. Mejia-Bernal JR, Gómez-Solís C, Juárez-Ramírez I, Ortiz-Rabell G, Díaz-Torres LA. Photocurrent generation using ZnO/CuO/Ag heterojunction films. *J. Mater. Sci. Mater. Eng.* **20**, 38 (2025). https://doi:10.1186/s40712-025-00217-8.